ORIGINAL ARTICLE

Development of hardware neural networks generating driving waveform for electrostatic actuator

Takuro Sasaki[1] · Mika Kurosawa[1] · Masaya Ohara[1] · Yuichiro Hayakawa[1] · Daisuke Noguchi[1] · Yuki Takei[1] · Minami Kaneko[1] · Fumio Uchikoba[1] · Ken Saito[1]

Abstract

The authors are studying to control the locomotion of the microrobot system using hardware neural networks (HNN). In previous research, a waveform generator was used to drive the electrostatic actuators of the microrobot. Once the driving circuit is constructed using HNN, the controlling circuit and the driving circuit can be integrated into a single chip. In this paper, the authors will propose the driving circuit using HNN. The HNN consists of two self-oscillating cell body models, six separately-excited cell body models, four excitatory-synaptic models, and six inhibitory-synaptic models. The single self-oscillating cell body model outputs the electrical oscillated square waveform as 3 MHz of frequency. The proposed HNN generates a long delay without using large capacitors. As a result, the proposed HNN can generate the driving waveform of electrostatic actuators with variable frequency. The frequency of the driving waveform could vary from 50 to 100 Hz. Also, the proposed HNN connected to the Central Pattern Generator (CPG) model. The CPG model with proposed HNN outputs the driving waveform of the electrostatic actuator which can perform the tripod gait pattern of the microrobot.

Keywords Microrobot · MEMS · Electrostatic actuator · Hardware neural networks

1 Introduction

In recent years, interest in developing the robot system using artificial intelligence (AI) and the internet of things (IoT) technology is increasing toward a realization of "Society 5.0". In particular, a microrobot focused on as a next-generation robot. The microrobots can take advantage of small bodies and can enter a small place where people cannot reach [1]. Also, multiple microrobots can use for collecting information about the environment widely and autonomously. However, a microrobot is challenging to minimize because of a power supply, sensors, a control circuit, and actuators that are difficult to make small. The actuator for microrobot is required to have a large displacement, a high-speed response, and low power consumption. The driving principle of micro actuators is various such as Electromagnetic, electrostatic [2], shape memory alloy,

✉ Takuro Sasaki
  csta19013@g.nihon-u.ac.jp

  Mika Kurosawa
  csmi19009@g.nihon-u.ac.jp

  Masaya Ohara
  csma18006@g.nihon-u.ac.jp

  Yuichiro Hayakawa
  csyu18023@g.nihon-u.ac.jp

  Daisuke Noguchi
  csda18020@g.nihon-u.ac.jp

  Yuki Takei
  csyk19002@g.nihon-u.ac.jp

  Minami Kaneko
  takato@eme.cst.nihon-u.ac.jp

  Fumio Uchikoba
  uchikoba@eme.cst.nihon-u.ac.jp

  Ken Saito
  kensaito@eme.cst.nihon-u.ac.jp

1 Nihon University, 7-24-1 Narashinodai, Funabashi, Chiba 274-8501, Japan

thermal expansion [3], and so on. Electromagnetic motors are high power and easy to control. Therefore, electromagnetic motors used for various industrial machines, precision machines, and robots. However, a downsizing under the millimeter size of electromagnetic motors is difficult because of the magnet and coil. Many researchers are researching and developing small size actuators based on new principles and functional materials. Due to the development of ceramics and manufacturing technology, the use of piezoelectric elements is expanding [4]. The piezoelectric element can generate a large force while having a small amount of displacement and can obtain responsiveness of several kHz. In recent years, miniaturization of electrostatic actuators done using micro electro mechanical systems (MEMS) technology [5–7].

In previous research, our constructed microrobot system succeeded to perform walking using external power supply [8, 9]. A shape memory alloy (SMA) actuator is used for driving the legs of the microrobot. SMA actuator has a large generating force and is simple and easy to miniaturize. However, the response speed was slow and the power consumption was high. Therefore, we developed an electrostatic actuator utilizing an inchworm mechanism as a new actuator [9]. Our proposed electrostatic actuator outputs more than 1.0 mN which is suitable for the motion of the microrobot's legs. Although the output is smaller than the SMA actuator, the electrostatic actuator has a small size (2.5×2.2 mm), low power consumption (1.0 mW) and fast response speed. By achieving a low power consumption of 60 V drive, the microrobot can also be driven by solar cells [9]. A square waveform from 50 to 100 Hz is required to drive the electrostatic actuator. In the previous research, the waveform generator has been used to generate the driving waveform of the electrostatic actuators. Therefore, integrated circuit (IC) chips which can generate the driving waveform of the electrostatic actuators are required to mount on the microrobot system.

In this paper, the authors will propose hardware neural networks (HNN) that can drive the electrostatic actuators. HNN consists of self-oscillating cell body models, separately-excited cell body models, excitatory-synaptic models, and inhibitory-synaptic models. The single self-oscillating cell body model outputs the electrical oscillated square waveform as 3 MHz of frequency. Usually, the large capacitor needs to output the low frequency such as 50–100 Hz. Therefore, the authors discussed how to generate a large delay without using large capacitors. Also, HNN needs to vary the output frequency. The authors made the variable frequency mechanism to the HNN.
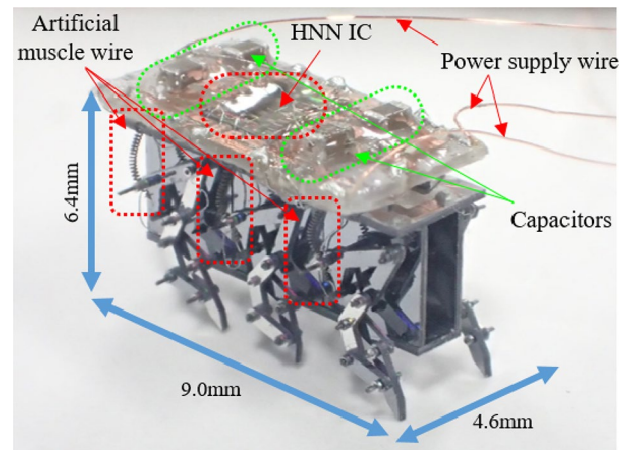

Fig. 1 Microrobot system [8]

Table 1 Specification of the helical type artificial muscle wire

Standard coil diameter (mm)	0.2
Wire diameter (mm)	0.05
Practical maximum force produced (gf)	3–5
Kinetic displacement (%)	50
Standard drive current (mA)	50–100
Standard electric resistance (Ω/m)	3600

2 Microrobot

Figure 1 shows our previously proposed microrobot system [8]. Each part manufactured by MEMS technology. The microrobot has a width of 4.6 mm, a height of 6.4 mm, and a length of 9.0 mm. The weight of the microrobot was 162 mg. An IC chip mounted on the robot can generate a gait pattern of the microrobot. Table 1 shows the basic characteristics of the SMA actuator that drives the microrobot. The power consumption to actuate a single leg was 94 mW.

3 Electrostatic actuator

Figure 2 shows our previously proposed electrostatic actuator [9]. Figure 2a shows the picture of the electrostatic actuator. The size of the electrostatic actuator was 2.2×2.5 mm. The electrostatic actuator consists of two pairs of electrostatic actuators, a central shuttle, arms, sub-springs, and a main-spring. The arms transmit the force of the actuators. Sub-springs and main-spring return the shuttle to the primary position. The electrostatic actuator has three electrode pads, V_{D1}, V_{D2}, and GND. Figure 2b shows

Fig. 2 Electrostatic actuator (**a**) Picture of the actuator (**b**) Generating force characteristic [9]
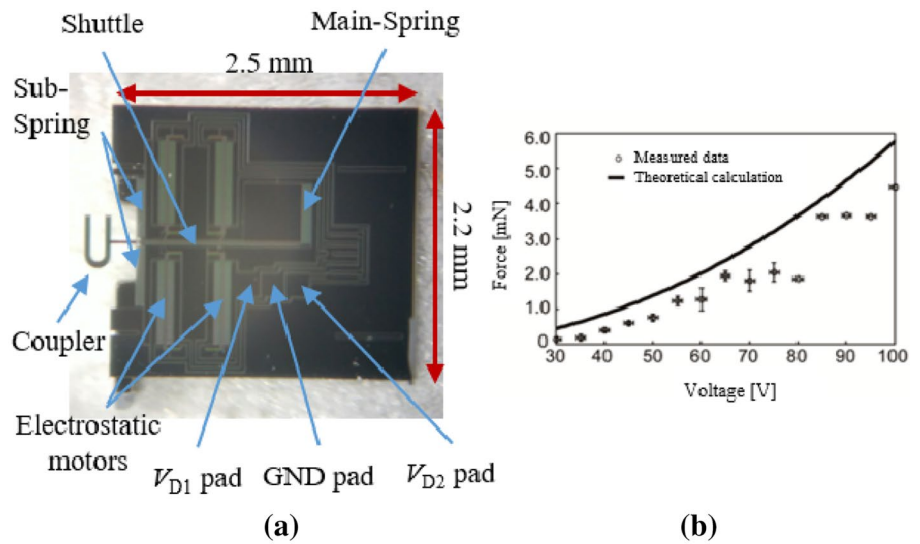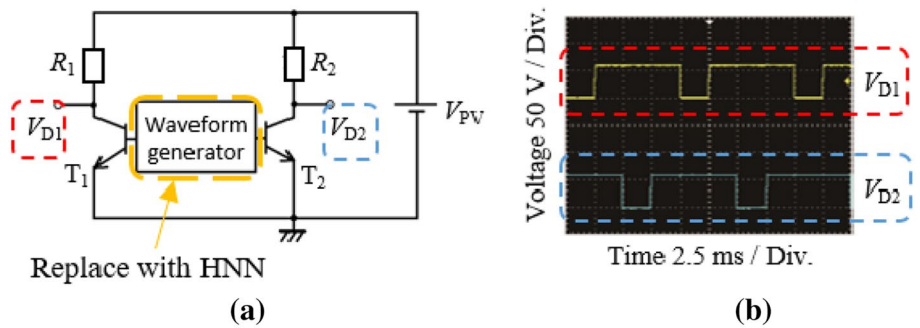

(a)

(b)

Fig. 3 Driving circuit of electrostatic actuator (**a**) Circuit diagram (**b**) Driving waveform [9]

(a)

(b)

the generating force characteristics of the electrostatic actuator. The solid line shows the theoretical calculation where an open circle indicates the measured data. This figure shows that an output of more 1.0 mN can obtain at 60 V. The generating force is suitable for the motion of microrobot.

Figure 3 shows the driving circuit of the electrostatic actuator. Figure 3a shows the circuit diagram of the driving circuit. The circuit parameters are $R_1 = R_2 = 2.2$ MΩ, $V_{PV} = 60$ V. The driving waveform shown in Fig. 3b is generated by a waveform generator which is a square wave with a pulse width of 7.5 ms, a pulse period of 10 ms, and a pulse amplitude of 60 V. The authors will replace the waveform generator to HNN in this paper.

4 Hardware neural networks

4.1 Basic components

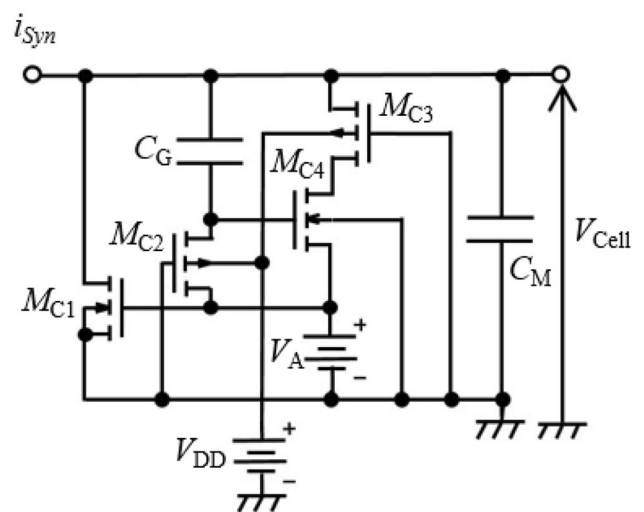In previous research, the authors constructed CMOS circuit based hardware neuron models with which can simulate the
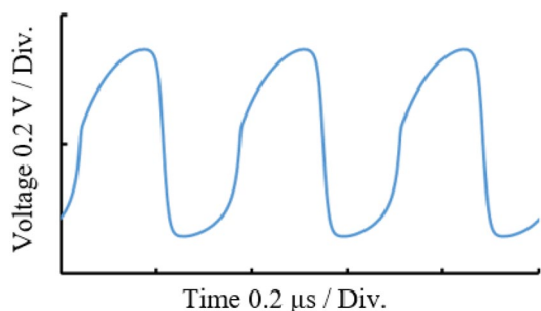

Fig. 4 Circuit diagram of the cell body model [11]

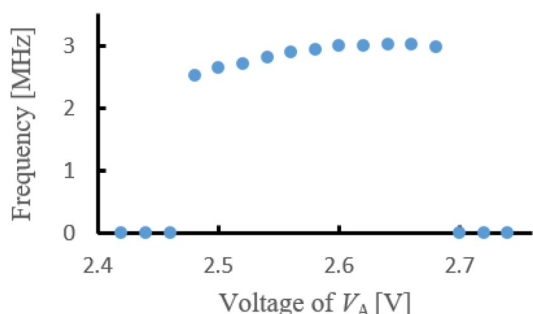**Fig. 5** Example of output waveform of the cell body model (self-excited oscillating mode)

Fig. 6 Frequency characteristic of cell body model (self-excited oscillating mode)

Fig. 7 Circuit diagram of synaptic model [11]
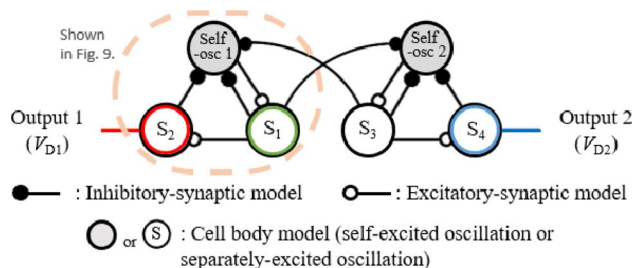
Fig. 8 Schematic diagram of the HNN

characteristics of biological neurons [10]. Each component of the HNN described in this chapter.

Figure 4 shows the circuit diagram of the cell body model. The circuit consists of capacitors: C_G, C_M, MOSFET: M_{C1}, M_{C2}, M_{C3}, M_{C4}, voltage source: V_A, V_{DD}.

The cell body model is an oscillation circuit that outputs pulses as shown in Fig. 5. Figure 5 shows the waveforms when the circuit parameters are as follows: $C_G = 1$ pF, $C_M = 0.1$ pF, $M_{C1} = $ W/L $= 1.2$ μm/8.5 μm, $M_{C2} = 1.2$ μm/10 μm, M_{C3}, $M_{C4} = 10$ μm/1.2 μm, $V_A = 2.6$ V, $V_{DD} = 2.0$ V. The frequency is 3.0 MHz.

Figure 6 shows a frequency characteristic of the cell body model in the condition of self-excited oscillating mode. The cell body model outputs pulses as in the range of 2.48–2.68 V. The cell body model switches to separately-excited oscillation mode by lowering V_A to 0.5 V.

Synapse is a connection part between the cell body. Figure 7 shows the circuit diagram of the synaptic model. The synaptic model consists of MOSFET: M_{S1}, M_{S2}, M_{S3}, M_{S4}, M_{E5}, M_{E6}, M_{E7}, M_{I1}, capacitor: C_S, voltage source: V_{DD}, V_{int}. The synaptic model mimics the characteristics of the biological synapse. In Fig. 7, "i_E" is transmitted as a signal by an excitatory synaptic model to the post-cell body model. By connecting the excitatory synaptic model, the pre-cell body model excites the post-cell body model. Therefore,
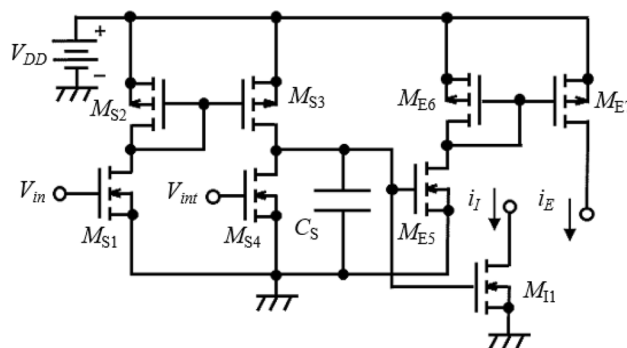
both cell body models will oscillate with in-phase synchronization. On the other hand, "i_I" is transmitted as a signal by the inhibitory synaptic model to the post-cell body model. The inhibitory synaptic model inhibits the oscillation of the post-cell body model. Therefore, both cell body models will oscillate with anti-phase synchronization.

4.2 Constructed hardware neural networks

Figure 8 shows the schematic diagram of the constructed HNN. If the self-oscillating cell body model (Self-osc 1) is not connected with the other cell body model, the Self-osc 1 oscillates at 3.0 MHz such as shown in Fig. 5. The separately-excited oscillation cell body model S_1 and S_2 are the delay circuit. The delay mechanism is as follows.

1. Self-osc1 oscillates a pulse.
2. A pulse of Self-osc1 excites the S_1.
3. S_1 oscillates a pulse.
4. A pulse of S_1 inhibits the Self-osc1. It also excites the S_2.
5. S_2 oscillates a pulse.
6. A pulse of S_2 inhibits the Self-osc1.

As a result, Self-osc 1 could not oscillate a pulse during the inhabitation from S_1 and S_2. Also, S_1 and S_3 inhibit
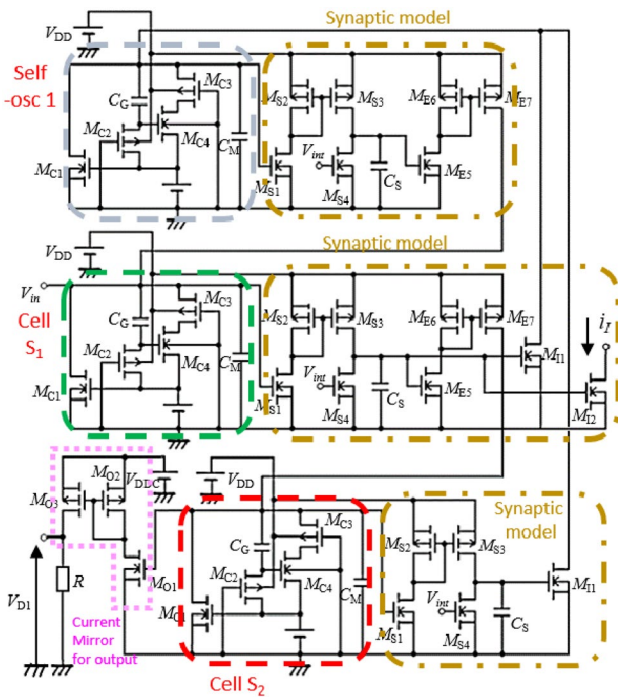
Fig. 9 Circuit diagram of HNN (Left part of Fig. 8.)

Fig. 10 Layout pattern of the HNN

Self-osc 1 and Self-osc 2, respectively. Thus, the output of HNN V_{D1} and V_{D2} will be an anti-phase waveform.

Figure 9 shows the circuit diagram of the HNN (Left part of Fig. 8). The circuit diagram shows only Output $1(V_{D1})$ by the self-oscillating cell body model 1, the separately-excited oscillation cell body model S_1, and S_2. The circuit parameter is as follows. MOSFET: $M_{C1} = 1.2$ μm /8.5 μm, $M_{C2} = 1.2$ μm/10 μm, $M_{C3}, M_{C4} = 10$ μm /1.2 μm, $M_{S1}, M_{S2}, M_{S3}, M_{S4}, M_{E5}, M_{E6}, M_{O2}, M_{I1}, M_{I2} = 10$ μm /10 μm, $M_{E7} = 2$ μm /10 μm, $M_{O1} = 20$ μm /2 μm, $M_{O3} = 20$ μm /2 μm, capacitor: $C_G = 1$ pF, $C_M = 0.1$ pF, $C_S = 8$ pF, resistance: $R = 5$ kΩ, Power-supply voltage: $V_{DDC} = 6.0$ V, $V_A = 2.6$ V, $V_{DD} = 2.0$ V, $V_{AS} = 500$ mV, $V_{int} = 510$ mV.

A current mirror circuit is arranged at the output of the separately excited oscillation cell body model S_2. The current mirror circuit is for the output circuit.

4.3 Layout

Figure 10 shows a layout pattern of the HNN. A red dotted line shows the constructed HNN, where the other part is the test element. The size of an IC chip is 2.5×2.5 mm. Twenty electrode pads are used as V_A, V_{AS}, V_{DD}, V_{DDC}, V_{int}, V_{D1}(output 1), V_{D2}(output 2), and GND for the created network part. This figure shows the HNN could be constructed in the IC chip.
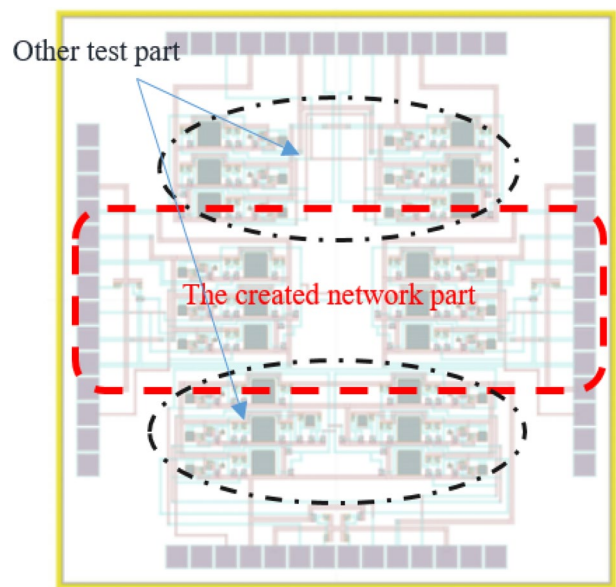
4.4 HNN with central pattern generator model

In previous research, the authors developed the Central Pattern Generator (CPG) model for mounting on the microrobot [12]. CPG produces gait patterns of living organisms. The tripod gait pattern is the most typical gait of insects. In this paper, the CPG model used for outputting tripod gait patterns. Figure 11 shows a schematic diagram of the CPG model.

A self-oscillating cell body model C_1 and S_1 connected each other by a NOT circuit with the excitatory synaptic model. Thus, the inverted C_1 output waveform and S_1 output waveform synchronous. Also, the output waveform of S_1 inverted by the NOT circuit. Therefore, the HNN outputs a two-phase waveform according to the output waveform of each cell body models of C_1–C_6.
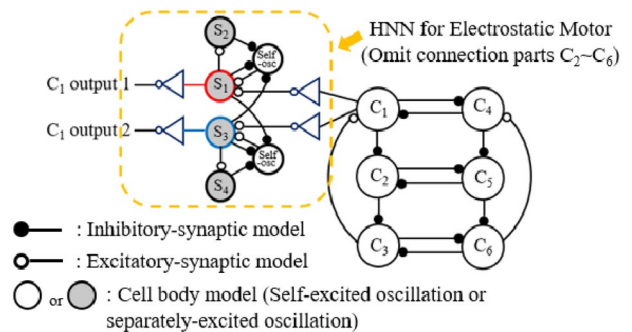

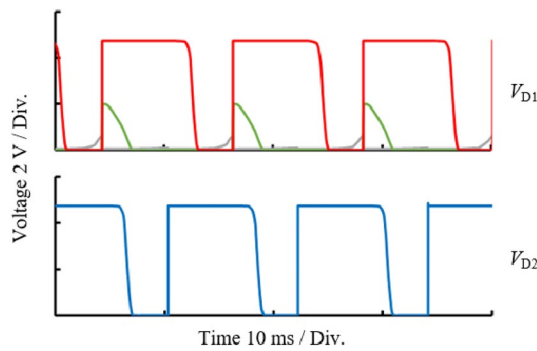**Fig.11** Schematic diagram of CPG connected the HNN
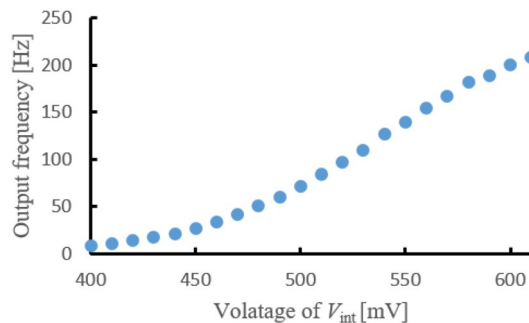
Fig. 12 Example of generated driving waveform of HNN

Fig. 13 Output-frequency characteristic of HNN (Varying V_{int})

Fig. 14 Output-frequency characteristic of HNN (Varying C_S)
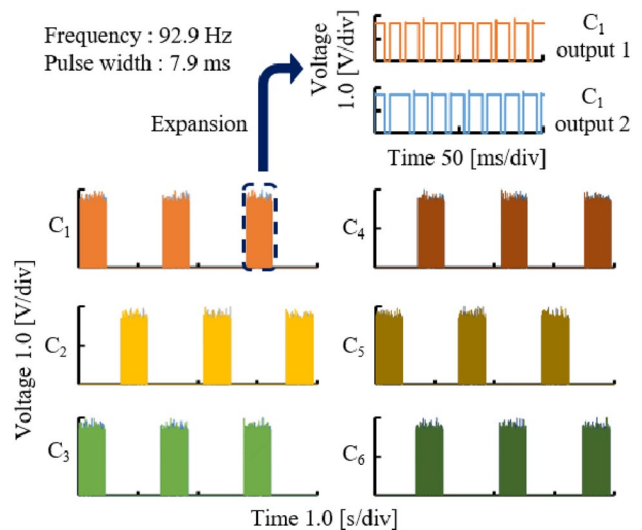
Fig. 15 An example of tripod waveform by CPG connected the HNN

5 Simulation result

Figure 12 shows the example of a generated driving waveform of HNN. The simulation was done using HSPICE. Three waveforms of the Self-osc 1 (gray), the S_1 (green), and S_2 (red) are shown for V_{D1}. Only the S_4 (blue) is shown for V_{D2}.

The characteristics in the case of changing the parameters of the synaptic model are shown as follows. An output-frequency characteristic of HNN by varying V_{int} is shown in Fig. 13. The output frequency increases by increasing V_{int}.

Figure 13 shows our constructed HNN can change the speed of the actuation of the electrostatic actuator. The synaptic model causes the frequency change (See Fig. 7, 8, 9). The frequency can adjust by the time constant of the RC integrator. RC integrator consists of the capacitor C_S and the MOSFET M_{S4}. In this paper, the frequency changed by varying the gate voltage V_{int} of MOSFET M_{S4}. Therefore, the frequency change can be in real-time.

Figure 14 shows an output-frequency characteristic of HNN by varying C_S. By increasing the capacity of C_S, the pulse width becomes longer and the frequency decreases. Even with such a change, the form of the pulse does not change, and the duty ratio is 0.6–0.7. According to Fig. 14, the authors fix the circuit parameter of C_S as 8 pF.
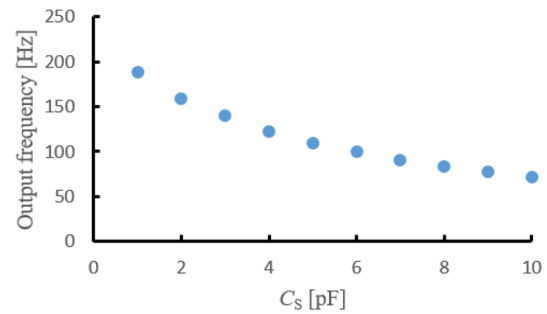
Figure 15 shows an example of a tripod waveform by proposed HNN connected to the CPG model. Figure 15 shows the CPG model with proposed HNN outputs the driving waveform of the electrostatic actuator which can perform the tripod gait pattern of the microrobot.

6 Conclusion

In this paper, the authors developed the driving circuit using HNN for driving the electrostatic actuator. The HNN generated a large delay without using large capacitors. The HNN generated the driving waveform of the electrostatic actuator with variable frequency. The frequency of the driving waveform could vary from 50 to 100 Hz. Also, we discuss the CPG model with proposal HNN outputs the driving waveform of the electrostatic actuator which can perform the tripod gait pattern of the microrobot.

In the future, the authors will propose the microrobot system using the electrostatic motor.

References

1. Saito K, Takato M, Sekine Y (2012) Biomimetics micro robot with active hardware neural networks locomotion control and insect-like switching behaviour. In: Proceedings of the 2009 international joint conference on neural networks, Atlanta, Georgia, USA, pp 2748–2755

2. Kuroki J, Shinshi T, LichuanLi L et al (2006) Micro-magnetic bearing motor (in Japanese). J Jpn Soc Precis Eng 72–5(2006):662–667

3. Zeng Z, Jin H, Zhang L et al (2014) Low-voltage and high-performance electrothermal actuator based on multi-walled carbon nanotube/polymer composites. Carbon 84(2015):327–334

4. Maeda H, Tani K, Suzuki M, Suzuki Y et al (1998) Development of piezoelectric micromotor (in Japanese). Horolog Inst Jpn 42–4(1998):31–39

5. Sakata M, Komura Y, Seki T et al (1999) Micromachined relay which utilizes single crystal silicon electrostatic actuator, technical digest. In: IEEE international MEMS 99 conference. Twelfth IEEE international conference on micro electro mechanical systems, Orlando, FL, USA, 21 Jan 1999

6. Fujita H, Actuators M (1988) J Jpn Soc Precis Eng 54–9:13–18

7. Higuchi T (2002) Prospect of micro actuators. J Jpn Soc Precis Eng 68–5:629–632

8. Kawamura S, Tanaka D, Tanaka T et al (2018) Neural networks IC controlled multi-legged walking MEMS robot with independent leg mechanism. Art Life Robot 23(3):380–386

9. Ken S, Contreras DS, Takeshiro Y et al (2018) Study on silicon device of microrobot system for heterogeneous integration. In: International conference on electronics packaging and iMAPS all Asia conference (ICEP-IAAC), Mie, Japan, 17–21 April 2018

10. Someya K, Shinozaki H, Sekine Y (1999) Pulse type hardware chaotic neuron model and its bifurcation phenomena. Neural Networks 12:153–161

11. Saeki K, Nihei D, Tatebe T, Sekine Y (2014) IC implementation of an interstitial cell-based CPG model. Analog Integr Circ Sig Process 81:551–559

12. Ohara M, Kurosawa M, Sasaki T et al (2019) Development of hardware neural networks ic with switchable gait pattern for insect-type microrobot, 2019 IEEE/SICE international symposium on system integration. Sorbonne Université, Paris, France, pp 663–668